2013 International Conference on Unmanned Aircraft Systems (ICUAS)
May 28-31, 2013, Grand Hyatt Atlanta, Atlanta, GA

A Hardware-in-the-loop Test Rig for Aerial Manipulation

Christopher Korpela, Matko Orsag, Youngbum Jun, Pareshkumar Brahmbhatt, and Paul Oh

Abstract— **A hardware-in-the-loop test rig is presented to bridge the gap between basic aerial manipulation research and the ability of flying robots to perform tasks such as door opening, bridge repair, agriculture care, and other applications requiring interaction with the environment. Unmanned aerial vehicles have speed and mobility advantages over ground vehicles and can operate in 3-dimensional workspaces. In particular, the usefulness of these capabilities is highlighted in areas where ground robots cannot reach or terrains they are unable to navigate. However, most UAVs operating in near-earth or indoor environments still do not have the payload capabilities to support multi-degree of freedom manipulators. We present a rotorcraft emulation environment using a 7 degree of freedom manipulator. Since UAVs require significant setup time and to avoid potential crashes, our test and evaluation environment provides repeatable experiments and captures reactionary forces experienced during ground interaction. Our preliminary results indicate that we can accurately model, emulate, and control our aircraft-manipulator system during both arm actuation and interacting with target objects.**

I. Introduction

Expanding the workspace from 2-dimensions to 3-dimensions achievable only by air vehicles would greatly enhance the utility of flying robots with arms. A simple task such as replacing a light bulb requires a hydraulic lift if the socket is 2 stories or higher. A ground robot would have great difficulty performing this bulb replacement. However, a flying robot with a dexterous arm could easily approach the ceiling, hover, remove the old bulb, and insert the new one. Advantages of aerial manipulators have been explained in recent publications [1]–[8]. While still largely underdeveloped, aerial manipulation has seen advances in quadrotors and small co-axial helicopters. These vehicles are inexpensive and easy to operate in motion capture volumes and outdoor environments. However, manipulation capabilities are limited to grasping lightweight objects primarily due to the poor payloads of small UAVs (unmanned aerial vehicles).

Thus, the critical gap in aerial manipulation continues to be the inability to characterize reactionary forces and torques and the impact of those reactions transmitted back to a 6-DOF (degree of freedom) flying robot with one or more arms. Advances in aircraft payloads and developments in light-weight arms signal a positive trend toward dexterous aerial manipulation. Payload limitations will most likely not represent the limiting issue but rather how arm trajectories and ground interactions produce forces and torques on the aircraft. To bridge this gap, we propose a hardware-in-the-loop test rig to emulate aircraft dynamics and to perform dexterous manipulation from an aircraft-arm system.

Fig. 1: MM-UAV Test Rig with 7-DOF Manipulator

This paper presents a test rig incorporating the dynamic and kinematic model (Sec. III) for a mobile manipulating unmanned aerial vehicle, dubbed MM-UAV, as shown in Fig. 1. This model is applied to both simulation and hardware (Secs. V and VI) to characterize and compensate for reactionary forces. The end-effector pose for the arm is a combination of the six DOFs of the emulated aircraft, seven DOFs of the manipulator, and four DOFs for the hand for a total of 16 degrees of freedom. The aerial manipulation system presented in this paper can successfully manipulate and transport various objects while maintaining stable flight.

II. Concept of Operations

We envision MM-UAV performing similar tasks as existing ground robots, but with a higher degree of autonomy, speed, and mobility. Possible vehicles include duct-fan rotorcraft, standard or co-axial helicopters, and quadrotors containing multiple manipulators. For example, MM-UAV could perform bridge repair that is difficult for a human to reach or provide service-oriented functions for elderly or disabled persons. With multiple arms, MM-UAV could perch or grab on to a stationary object for added stability. Not limited to near-earth environments, this concept readily applies to underwater operations such as oil-rig repair or in space when interacting with satellites. Space robots typically focus on capturing free-floating objects with unknown inertial and dynamic properties. In an MM-UAV paradigm, the goal is to dexterously manipulate non-floating objects in near-earth

Manuscript received May 1, 2013. This project was supported in part by a US NSF CRI II-New, Award # CNS-1205490, DoD Advanced Civil Schooling, and a U.S. Fullbright Scholarship.

C. Korpela, Y. Jun, P. Brahmbhatt, and P. Oh are with the Drexel Autonomous Systems Lab, Drexel Univeristy, Philadelphia, PA 19104 USA {cmk325, yj55, pkb471}@drexel.edu, paul@coe.drexel.edu

M. Orsag is with Faculty of Electrical Engineering and Computing, University of Zagreb, 10000 Zagreb, Croatia morsag@fer.unizg.hr

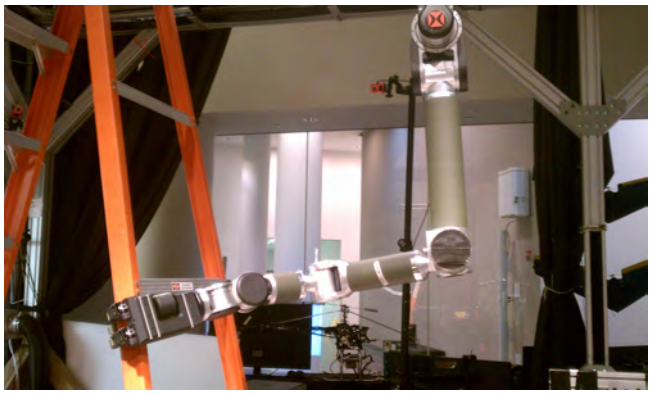

(a) Grabbing onto a support rail

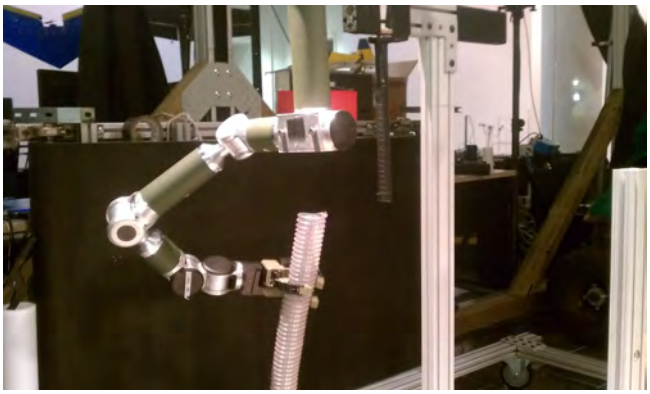

(b) Hose insertion

Fig. 2: Example MM-UAV Operations

environments such as inserting objects into walls, cutting tree branches, or turning door handles. Thus, there are many similarities between space robotics and aerial manipulation. Figs. 1 and 2 illustrate a few concept applications for this research.

III. System Approach and Modeling

A. Mobility

Rotary-wing aircraft come in various configurations to include but not limited to a standard helicopter with a main rotor and tail rotor, co-axial helicopters, duct-van systems, and quadrotors. Rotorcraft have the ability to hover and can easily navigate near-earth and indoor environments as compared to their fixed-wing counterparts. Since UAVs require significant setup time, suitable testing locations, and can be significantly damaged in crashes, a 3-axis two-story overhead gantry (Fig. 3) is utilized to provide linear and rotational displacement and velocities for the modeled aircraft. This test environment enables the capture of forces and torques transmitted to the aircraft. Dubbed MM-SISTR (Mobile Manipulating-SISTR), the gantry system is modeled after the Systems Integrated Sensor Test Rig (SISTR) [9]. SISTR was developed as a hardware-in-the-loop test rig and designed to be used to evaluate obstacle detection sensors (LIDAR, computer vision, ultrasonic, ultra-wideband radar, millimeter wave radar, etc.), design sensor suites, and test collision avoidance algorithms. The gantry can traverse 0.35 m/s along each x, y, and z axis. To provide yaw, pitch, and roll angles and velocities for the emulated aircraft, a 3-DOF gimbal is attached to the gantry z-axis. MM-SISTR can be tuned for almost any rotorcraft model.

For this particular analysis, a quadrotor model was chosen due to their simplicity in mechanical operation and the symmetry of their construction. The standard right-handed earth inertial reference frame is denoted as $E = \{E_x, E_y, E_z\}$ and $B = \{B_x, B_y, B_z\}$ denotes the vehicle body fixed reference frame. The position of the vehicle's center of mass is $\xi = (x, y, z)^T$ *w.r.t.* the inertial frame rotated by $R \in SO(3)$. The vehicle orientation *w.r.t.* the inertial frame is denoted as $\eta = \{\psi, \theta\, \phi\}$ where yaw, pitch, and roll are the Euler angles, respectively. The Newton-Euler formation for the rigid-body dynamics is [10]

$$\dot{\xi} = v \tag{1a}$$

$$m\dot{v} = R_{E_z} F - mgE_z \tag{1b}$$

$$\dot{R} = R\hat{\Omega} \tag{1c}$$

$$I\dot{\Omega} = -\Omega \times I\Omega + \tau \tag{1d}$$

where m, I, v, and Ω represent the mass, interia matrix, linear velocity, and angular velocity of the vehicle, respectively. F and τ are the forces and moments from the rotors applied to the vehicle body.

This research incorporates manipulator dynamics and the

Fig. 3: MM-SISTR overhead gantry, gimbal, and manipulator

dynamics of the quadrotor. Due to the resulting complexity of the model and mission requirements, the quadrotor dynamics considered in this paper do not account for various aerodynamic effects (i.e. blade flapping, ground effect, etc.) experienced during highly dynamic flying maneuvers. Most of the missions require stable hovering maneuvers, which justifies a simplified mathematical model without accounting for the previously mentioned aerodynamic effects. As the manipulator dynamics are introduced through the recursive Newton-Euler method in Sec. III-B, it is possible to separate and model the quadrotor motion based on Newton-Euler equations for rigid body translation and rotation [11]. The mass, moments of inertia, and dynamic movement of the manipulator are then introduced as disturbances to the quadrotor model.

Using Model Reference Adaptive Control (MRAC), a linearized model of the aircraft serves as the reference model. The gains are updated according to the difference between the error of the gantry states and the math model of the rotorcraft. To satisfy global asymptotic stability, the following Lyapunov candidate function is implemented:

$$V = e^T P e + \Phi^T \Gamma^{-1} \Phi \tag{2}$$

were e is the error between the states of the reference model and the gantry dynamics, P is the positive definite matrix of the Lyapunov equation, Φ is the controller gain vector and Γ is a diagonal matrix whose diagonals are the relative gain update rates.

B. Manipulation

1) Manipulator Kinematics: As shown in Fig. 4, the redundant 7-DOF manipulator consists of serially connected revolute, rigid, and modular joints and links. Frame 0 is located at the base of the torso while Frame *E* is the end-effector frame. Joint rotation positions are also indicated. The Denavit-Hartenburg parameters are shown in Table I. The assembly consists of a torso with the option for two manipulators. The current configuration consists of the left arm only containing the following joints: should pitch, shoulder roll, shoulder yaw, elbow pitch, wrist yaw, wrist pitch, and wrist roll. The 4-DOF left arm end-effector has joints: thumb roll, thumb pitch, middle finger pitch, and index finger pitch. The distal joints of the fingers are under-actuated and conform to the object being grasped. This arm has a load capacity of over 50 pounds (23 kg) but only weighs 16 pounds (7.3kg) making it easily transportable by an autonomous helicopter.

The transformation matrix relating the torso to the end-effector frame is obtained by chain-multiplying the homogeneous transformations together where joint 'i' is in the standard form:

$$^{i-1}T_i = \begin{bmatrix} c_{\theta_i} & -s_{\theta_i} c_{\alpha_i} & s_{\theta_i} s_{\alpha_i} & a_i c_{\theta_i} \\ s_{\theta_i} & c_{\theta_i} c_{\alpha_i} & -c_{\theta_i} s_{\alpha_i} & a_i s_{\theta_i} \\ 0 & s_{\alpha_i} & c_{\alpha_i} & d_i \\ 0 & 0 & 0 & 1 \end{bmatrix} \tag{3}$$

The position vector of the end-effector can easily be obtained through forward kinematics. The complete transformation from base to end-effector can be simplified as:

$$^0H_n = \begin{bmatrix} R_n^0 & T_n^0 \\ 0...0 & 1 \end{bmatrix} \tag{4}$$

where R_n^0 represents the 3 x 3 rotated orientation and T_n^0 is the 3 x 1 position of the tool with respect to the base frame.

2) Inverse Kinematics: Given a desired task space trajectory $(x(t), \dot{x}(t))$, the goal is to find a suitable joint space trajectory $(q(t), \dot{q}(t))$ to generate the given trajectory. The literature has numerous examples of geometric, numerical, and analytical methods to solve the inverse kinematic (IK) problem. Due to the inherent drift in the aircraft, the system will continually require fast IK computations. Therefore, we have chosen an analytical IK approach.

The IK solver (called *ikfast*) is a closed-form process that can generate solutions on the order of 4 microseconds which is significantly faster than numerical methods [12]. Thus, it is possible to investigate the null space of the solution set. In a kinematically redundant manipulator, a nonempty null space exists because of the excess of input space relative to the manipulable space $(n > m)$. The null space is a set of task space velocities that yield null joint space velocities

Fig. 4: CAD drawing of manipulator (showing each joint)

Frame	Link	θ	d	a	α
0-1	1	q_1	d_1	0.250	0
1-2	2	q_2	d_2	0.077	pi/2
2-3	3	q_3	d_3	0.242	0
3-4	4	q_4	d_4	0.077	pi/2
4-5	5	q_5	d_5	0.136	0
5-6	6	q_6	d_6	0.074	0
6-7	7	q_7	d_7	0.156	0
7-E	E	0	0	0	0

TABLE I: Denavit-Hartenberg parameters for the manipulator

at the current robot configuration and these task velocities belong to the orthogonal complement of the feasible task space velocities [13]. A key feature of the IK solver includes the generation of all possible 6D transform solutions. Further, it can handle arbitrary joint complexity and generates an optimized C++ database.

The Jacobian is used to linearly map the joint space and task space velocities. Therefore, the differential kinematics showing this mapping has the form:

$$\dot{x} = J(q)\dot{q} \tag{5}$$

The basic inverse solution to (5) is derived from the pseudoinverse J^t of the matrix J where the inverse solution has the form:

$$\dot{q} = J^{\dagger}(q)\dot{x} \tag{6}$$

and the pseudoinverse $J^{\dagger}$ can be computed as:

$$J^{\dagger} = J^T(JJ^T)^{-1} \tag{7}$$

A common method of including the null space in a solution is the formulation in [14] where:

$$\dot{x} = J^{\dagger}\dot{y} + (I - J^{\dagger}J)z, z \in R^n \tag{8}$$

3) Manipulator Dynamics: Using a recursive Newton-Euler algorithm [15], [16] and neglecting friction forces, one can derive generalized force/torque equations produced from each joint movement:

$$\sum_{j=0}^{n}[D_{ij}(\mathbf{q})\ddot{q}_j] + \sum_{k=0}^{n}\sum_{j=0}^{n}[C_{kj}^{i}(\mathbf{q})\dot{q}_k\dot{q}_j] + h_i(\mathbf{q}) = \tau_i, 0 \leq i \leq n \tag{9}$$

with D_{ij} as a generalized inertia tensor, C_{kj}^{i} is the generalized Coriolis and Centrifugal force matrix and h_i is a generalized gravity force.

Given that τ_0 calculates forces produced on the aircraft body (i.e. $w = \tau_0$), Newton-Euler analysis provides the necessary tools to calculate static and dynamic disturbances acting on the rotorcraft. In a complete model, Newton-Euler equations for manipulator motion need to be provided with initial angular and linear speeds and accelerations. To simplify the overall problem, we make a reasonable assumption that the aircraft is in hover during manipulation. This assumption enables us to regard the initial linear and angular dynamics of the aircraft body as zero, thus effectively decoupling the dynamics.

C. Feedback

The primary pose estimator is a motion capture system based on 18 V100:R2 OptiTrack cameras connected to a PC running Arena Software. The PC sends the data via the NatNet protocol. The controller PC implements a C++ class to read in the data being streamed from the motion capture computer. Fast Ethernet speed allows for a fast connection with practically no lag between sending and receiving data. Table II shows the parameters of the motion capture system. Motion capture provides pose information for the gantry z-axis (emulated aircraft) and other rigid bodies such as target objects.

MOCAP Data			
Number of Cameras	Refresh Rate	Pos. Resolution	Speed Resolution
18	10 Hz	1 mm	0.1 m/s

TABLE II: OptiTrack Motion Capture System Data

The overhead gantry has position encoders to calculate travel distance and velocity for each axis. Velocity commands and encoder updates are sent over UDP. For the 3-DOF gimbal and 7-DOF manipulator, each actuator has local velocity, position, force, and impedance loop closure. Communications are provided over Ethernet through a UDP to CAN bus bridge. Considerable effort has been made to implement the control system using the Robot Operating System (ROS). Using the provided node based and message exchange system, it is easy to build the control system and establish communications between the manipulator and gantry test rig.

IV. Impedance Control

An impedance control strategy is proposed to control the dynamic interaction between the manipulator and its environment. Impedance control enables contact between the manipulator and its environment while maintaining stability during the transition from free motion to interaction [17]. In a simplified manner, the manipulator can be seen as a mass-spring-damper system behaving like an impedance towards the environment. Even with excellent vehicle position control, relative motions between the UAV and work piece highlight the need for compliant manipulation approaches.

MM-SISTR emulates the behavior of a rotorcraft which is free-flying and easily influenced by moments caused by contact forces which could result in a crash. In addition, the manipulator is position and velocity controlled with high joint stiffness. As a result, the contact force at the end-effector of the manipulator is directly acting on the body of the aircraft as an angular moment. A Cartesian impedance control strategy [18]–[20] is proposed for manipulation. The manipulator is modeled as a single point mass and follows a given end-effector trajectory to manipulate an object. The force-torque sensor at the wrist measures the reactionary

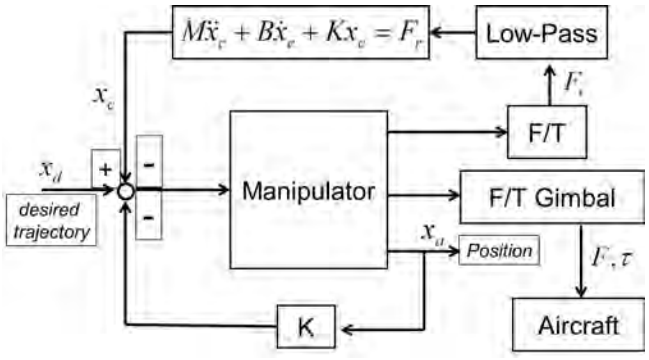

Fig. 5: Design concept for manipulator impedance control

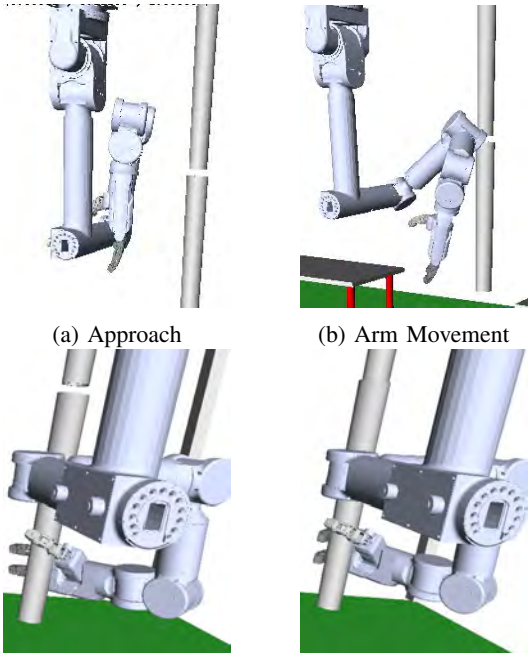

(a) Approach (b) Arm Movement

(c) Grasp (d) Insertion

Fig. 6: Images from hose-insertion simulation

force from interaction. The Cartesian impedance model is

$$M\ddot{x} + B\dot{x} + Kx = -F_r \tag{10}$$

where M, B, K are mass, damping, and stiffness coefficients, respectively, and F_r denotes the reaction force in contact.

The control objective is to minimize the unexpected impulsive force experienced by the hovering aircraft while tracking the given trajectory. In this case, the damping coefficient is the dominant parameter, the stiffness is very small, and the mass can be ignored. The damping value is then determined based on the hovering frequency and magnitude; low damping is appropriate for rapid movement but could be unstable, conversely, high damping is stable but not suitable for fast movement. With the proper impedance model, the trajectory is refined corresponding to the output response of the model. Fig. 5 shows the impedance control block diagram. The force including the impulsive contact force measured by the F/T (force/torque) sensor on the wrist is filtered out via a low pass filter. The data from the F/T sensor located in the base of the manipulator provides feedback to the aircraft controller for stabilization.

V. Simulation

The simulation environment consists of a full scale replica of MM-SISTR. The OpenRAVE [12] robotics virtual environment is used to simulate the aircraft-manipulator model for hose insertion. In this scenario, the manipulator grasps onto a hose (represented by a simple cylinder with similar mass properties) and inserts the hose into a replacement pump (represented by another cylinder). There is 5mm of clearance for the insertion. The manipulator is exported from CAD into a COLLADA format which is an XML schema that OpenRAVE supports. The *ikfast* solver generates the inverse kinematics solution based on the COLLADA file and IK type (Transform6D). A Python script is run to execute the necessary tasks to perform the hose insertion. First, the gantry joints are set as active to move the manipulator into position. Next, the end-effector grasps the hose after generating an IK solution. Finally, the hose is inserted into the pump after another IK solution is generated and executed. When a trajectory is computed, the planner must check for mechanical constraints that do not prevent arm movement, there are no environmental collisions, and finally there are no self-collisions.

VI. Experimental Results

A. Test Setup

To validate the system model, testing on the actual hardware focused on establishing a torque profile for relevant joints during both arm articulation and interaction with the environment. The gantry is moved to the target area providing the maximum allowable reach for the manipulator and the gantry is set to hover. A PVC cylinder is pre-loaded into the end-effector and the arm is positioned to an initial pose for hose insertion. Shoulder, elbow, and wrist pitch motions provide the majority of the degrees of freedom. Joint torques are recorded for analysis during arm movement and while making contact with the insertion point. ROS-nodes provide real-time joint state data and actuator position and velocity control at 50 Hz. Gantry and gimbal position corrections are performed to reject the applied torques caused by the manipulator. The motion capture system runs on a separate PC to provide rigid body transform data of the gantry z-axis position and velocity.

B. Hose Insertion Tests

In this section, the results of arm articulation and cylinder to pump contact are presented. Analysis of arm movement is critical as different arm trajectories can produce large variations of effective torque on the aircraft. From the zero position with the arm stowed in a pose generating a minimal moment on the aircraft, the arm moves through a trajectory to move the end-effector just prior to contact with the pump. The next step involves shoulder and elbow pitch joint movement to perform the hose insertion. Fig. 7 shows the torque profile and measured velocity of a given trajectory for the elbow pitch joint. Body torque experienced by the aircraft is fed to the attitude control to maintain a stable hover. Snapshots showing the elbow joint following the trajectory and making contact are shown in Fig. 8.

VII. Conclusions

In this paper a test rig for aerial manipulation is presented. One of the primary goals of this research is to capture and compensate for reactionary forces applied to a rotorcraft during interactions with the environment. The system kinematics and dynamics have been applied to our controller implementation. Compliance control is paramount when using rigid

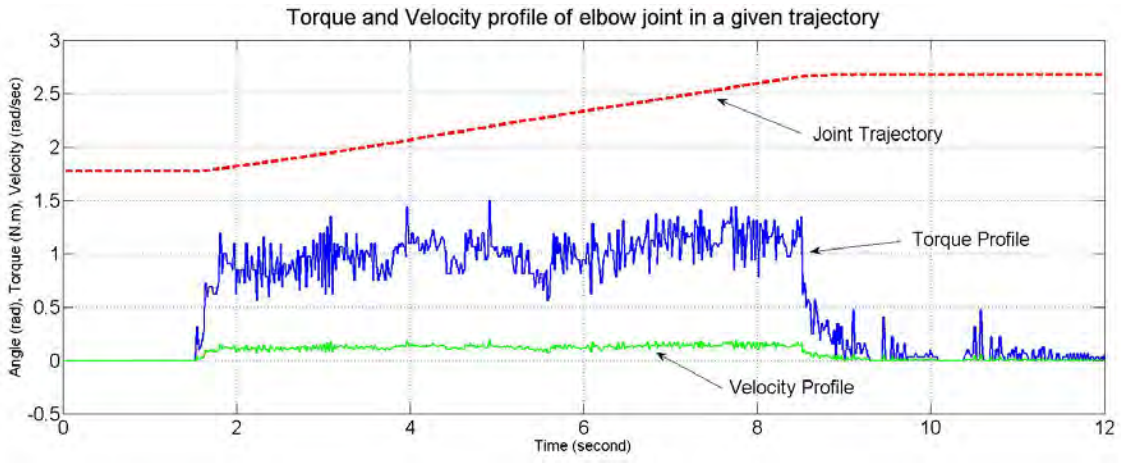

Fig. 7: Test Results showing elbow joint profile

(a) Approach (b) Arm Movement (c) Contact

Fig. 8: Torque profiling experiment

manipulators to ensure aircraft stability. Insertion-style tasks and simulation results confirm the kinematic and dynamic model and controller for the system. In the future, we plan to test different adaptive and robust control techniques in order to achieve greater flight stability and more dexterous manipulation.

REFERENCES

[1] M. Orsag, C. Korpela, and P. Oh, "Modeling and control of MM-UAV: Mobile manipulating unmanned aerial vehicle," in *Proc.International Conference on Unmanned Aircraft Systems, ICUAS*, 2012.

[2] A. Keemink, M. Fumagalli, S. Stramigioli, and R. Carloni, "Mechanical design of a manipulation system for unmanned aerial vehicles," in *Robotics and Automation (ICRA), 2012 IEEE International Conference on*, may 2012, pp. 3147 –3152.

[3] D. Mellinger, Q. Lindsey, M. Shomin, and V. Kumar, "Design, modeling, estimation and control for aerial grasping and manipulation," in *Proc. IEEE/RSJ Int Intelligent Robots and Systems (IROS) Conf*, 2011, pp. 2668–2673.

[4] P. E. I. Pounds, D. R. Bersak, and A. M. Dollar, "Grasping from the air: Hovering capture and load stability," in *Proc. IEEE Int Robotics and Automation (ICRA) Conf*, 2011, pp. 2491–2498.

[5] V. Ghadiok, J. Goldin, and W. Ren, "Autonomous indoor aerial gripping using a quadrotor," in *Intelligent Robots and Systems (IROS), 2011 IEEE/RSJ International Conference on*, sept. 2011, pp. 4645 – 4651.

[6] S. Bellens, J. De Schutter, and H. Bruyninckx, "A hybrid pose / wrench control framework for quadrotor helicopters," in *Robotics and Automation (ICRA), 2012 IEEE International Conference on*, may 2012, pp. 2269 –2274.

[7] A. Albers, S. Trautmann, T. Howard, T. A. Nguyen, M. Frietsch, and C. Sauter, "Semi-autonomous flying robot for physical interaction with environment," in *Robotics Automation and Mechatronics (RAM), 2010 IEEE Conference on*, june 2010, pp. 441 –446.

[8] www.airobots.eu.

[9] V. Narli and P. Y. Oh, "Hardware-in-the-loop test rig to capture aerial robot and sensor suite performance metrics," in *Proc. IEEE/RSJ Int Intelligent Robots and Systems Conf*, 2006, pp. 3521–3526.

[10] S. Bouabdallah, P. Murrieri, and R. Siegwart, "Design and control of an indoor micro quadrotor," in *Robotics and Automation, 2004. Proceedings. ICRA '04. 2004 IEEE International Conference on*, vol. 5, april-1 may 2004, pp. 4393 – 4398 Vol.5.

[11] H. Hahn, *Rigid Body Dynamics of Mechanisms: Theoretical basis*, ser. Rigid Body Dynamics of Mechanisms. Springer, 2002.

[12] R. Diankov and J. Kuffner, "Openrave: A planning architecture for autonomous robotics," Robotics Institute, Pittsburgh, PA, Tech. Rep. CMU-RI-TR-08-34, July 2008.

[13] B. Siciliano, L. Sciavicco, L. Villani, and G. Oriolo, *Robotics: Modelling, Planning and Control*, 1st ed. Springer Publishing Company, Incorporated, 2008.

[14] L. Y. Z. Z. Wang, J., "Inverse kinematics and control of a 7-dof redundant manipulator based on the closed-loop algorithm," in *International Journal of Advanced Robotic System*, 2010, pp. 1–12.

[15] P. Corke, "A robotics toolbox for MATLAB," *IEEE Robotics and Automation Magazine*, vol. 3, no. 1, pp. 24–32, Mar. 1996.

[16] R. Jazar, *Theory of Applied Robotics: Kinematics, Dynamics, and Control (2nd Edition)*. Springer, 2010.

[17] N. Hogan, "Impedance control: An approach to manipulation," in *Proc. American Control Conf*, 1984, pp. 304–313.

[18] L. Biagiotti, H. Liu, G. Hirzinger, and C. Melchiorri, "Cartesian impedance control for dexterous manipulation," in *Proc. IEEE Int. Conf. Intelligent Robots and Systems IROS '03*, Oct 2003.

[19] D. Ericson, M. Weber, and I. Sharf, "Contact stiffness and damping estimation for robotic systems," in *Int. Journal of Robotics Research*, 2003.

[20] K. Lee and M. Buss, "Force tracking impedance control with variable target stiffness," in *The International Federation of Automatic Control*, vol. 16, no. 1, 2008, pp. 6751–6756.